Femtosecond-Laser-Induced Nanocavitation in Water: Implications for Optical Breakdown Threshold and Cell Surgery

Alfred Vogel,[1,*] Norbert Linz,[1] Sebastian Freidank,[1] and Günther Paltauf[2,†]

[1]*Institute of Biomedical Optics, University of Lübeck, Peter-Monnik-Weg 4, 23562 Lübeck, Germany*

[2]*Institute of Physics, Karl-Franzens-University Graz, Universitätsplatz 5, 8010 Graz, Austria*

(Received 4 September 2007; revised manuscript received 2 November 2007; published 23 January 2008)

We determined the bubble radius R_{max} for femtosecond optical breakdown in water at 347, 520, and 1040 nm with an unprecedented accuracy ($\pm$ 10 nm). At threshold, R_{max} was smaller than the diffraction-limited focus radius and ranged from 190 nm to 320 nm. The increase of R_{max} with laser energy E_L is slowest at 347 nm, providing optimum control of cell surgery. Experimental results agree with a model of bubble formation in heated and thermoelastically stretched liquids. Theory predicts a threshold temperature $T_{th} \approx 168\,^{\circ}\mathrm{C}$. For $T > 300\,^{\circ}\mathrm{C}$, a phase explosion sets in, and R_{max} increases rapidly with E_L.

DOI: 10.1103/PhysRevLett.100.038102 PACS numbers: 87.80.−y, 47.55.dp, 52.38.Mf, 52.50.Jm

For various biological applications, it is essential to dissect or knock out subcellular structures with nanometer precision, and femtosecond (fs) lasers are widely used for this purpose, as reviewed in [1]. In a recent theoretical study, we identified disruption by plasma-mediated nanocavitation as working mechanism of cell surgery with tightly focused fs laser pulses at repetition rates up to $f \approx 1$ MHz, while for $f \gg 1$ MHz surgery was shown to be mediated mainly by free-electron induced chemical decomposition [1]. We assumed that the combination of heat and thermoelastic tensile stress produced by ultrashort laser pulses results in bubble formation when the kinetic spinodal limit of water [2] is exceeded. For pulses of 100 fs duration and 800 nm wavelength focused into water at a numerical aperture (NA) of 1.3, the threshold temperature was predicted to be as small as 151.5 °C, and the corresponding bubble radius to be only 65 nm. An experimental confirmation of these predictions is of great importance for selecting optimum parameters for cell surgery, because cavitation is the key mechanism for collateral damage, and bubbles produced by longer laser pulses are usually tens or hundreds of micrometers large [3–5].

From a more principle point of view, bubble formation defines the optical breakdown threshold in aqueous media by ultrashort laser pulses for which plasma luminescence is too weak to serve as breakdown criterion [1,6]. The occurrence of a phase transition within the liquid constitutes a sharp threshold that is correlated with a well-defined volumetric energy density. While for dielectric solids, in which breakdown leaves permanent marks, damage thresholds can be determined retrospectively, time-resolved measurements are required for aqueous media in which the minute bubble produced by a tightly focused fs pulse lives only a few tens of nanoseconds.

The present study provides data for the maximum bubble radius R_{max} as a function of laser pulse energy E_L for near-UV, visible and IR wavelengths. Experimental results are then compared with the model predictions.

To determine fs breakdown thresholds in transparent media, the laser pulses must be focused at a high NA (≥ 0.9) to avoid corruption of the results by nonlinear beam propagation altering the focal spot size [7,8]. This is difficult to realize without introducing spherical aberrations into the laser beam path that will lead to erroneous threshold values [9]. In the present study, we use water immersion microscope objectives built into the wall of a cuvette to provide diffraction-limited focusing conditions at high NA.

Previous investigations of fs optical breakdown in water [6,10] addressed the dynamics of bubbles produced by laser pulses with 1 μJ energy (6–10 times above threshold) that expanded to maximum radii of 45–100 μm. The aim of the present study is to determine bubble sizes close to threshold that are below the diffraction-limited resolution of the microscope objective used for bubble generation [1]. We use the scattering of a probe laser beam to determine the bubble oscillation time T_{osc} and deduce R_{max} from T_{osc}, which is the lifetime of the first cycle of the cavitating bubble [3–6]. Previously, scattering techniques have been used for the analysis of single bubble sonoluminescence and the early expansion phase of fs-laser-produced bubbles [10,11]. The bubble dynamics was deduced from the temporal evolution of the *intensity* of the scattering signal which involved calibration problems. Since we are only interested in R_{max}, we can avoid such problems by resorting to the theoretically known relationship between R_{max} and T_{osc}.

Figure 1 depicts the experimental setup. We focus either the fundamental wavelength (1040 nm) or the 2nd or 3rd harmonic (520 or 347 nm) of an amplified Yb:glass laser (1 kHz, pulse width 340 fs) through long-distance water-immersion objectives (Leica HCX APO L U-V-I) built into the wall of a water-filled cell. The rear entrance pupil of the objective (63x, NA = 0.9 or 40x, NA = 0.8) is overfilled to create a uniform irradiance distribution corresponding to an Airy pattern in the focal plane. Single laser pulses are

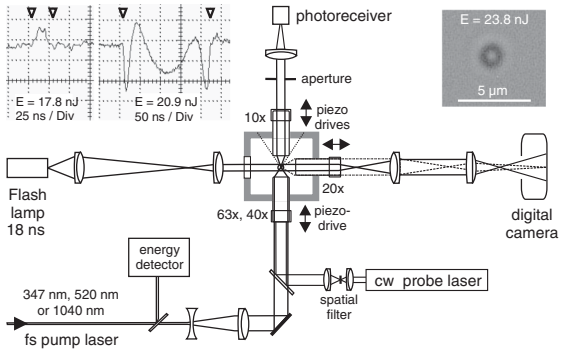

FIG. 1. Setup for the examination of fs laser-induced bubble formation in water. The insets show scattering signals (NA = 0.9) and a bubble photograph (NA = 0.8) for laser energies near threshold ($\lambda = 1040$ nm). Times of bubble generation and collapse are marked by arrowheads.

selected from the pulse train using a mechanical shutter. A spatially filtered cw probe laser beam (658 nm, 40 mW) is adjusted collinear and confocal with the fs beam. The transmitted probe light is collected by a 10x, NA = 0.3 water immersion objective and imaged onto an ac-coupled amplified photoreceiver (FEMTO, 25 kHz–200 MHz bandwidth) that is protected from the fs laser irradiation by blocking filters. When the bubble is much smaller than the focal diameter, its scattering signal is considerably weaker than the total amount of transmitted light. The ac coupling removes this bias and makes it possible to detect bubbles with only 15 ns oscillation time and 150 nm maximum radius with ± 10 nm accuracy.

To validate the scattering technique, larger bubbles are imaged with 1 μm optical resolution by a digital camera using a 20x, NA = 0.5 objective oriented perpendicular to the pump and probe beam axes. The object space is illuminated in Köhler technique using a plasma discharge lamp with 18 ns pulse duration. Confocal adjustment of all objectives can be achieved, when the 40x objective is used to focus the fs pulses.

The insets in Fig. 1 show a bubble photograph close to the resolution limit, and scattering signals for different pulse energies at the laser focus. The signals are complex, due to the rapidly changing Rayleigh and Mie scattering characteristics during bubble expansion and collapse [11] but $T_{\rm osc}$ can always be easily determined. For large bubbles, $R_{\rm max}$ can be calculated from $T_{\rm osc}$ using the Rayleigh formula [3,12]. However, for bubble sizes below a few micrometers the Rayleigh equation is not exact because it neglects surface tension that produces a pressure scaling with $1/r$ which adds to the hydrostatic pressure. Therefore, we calculated the relation between $T_{\rm osc}$ and $R_{\rm max}$ using the Gilmore model which considers surface tension [13]. In an additional step, we used our full model of fs-laser-induced bubble formation [1], taking also the temperature dependence of surface tension into account [14]. The Gilmore model well approximates the $R_{\rm max}(T_{\rm osc})$ relation provided by the full model, but the Rayleigh formula leads to a marked underestimation of the bubble size for $T_{\rm osc} < 1$ μs.

Figure 2 shows the dependence $R_{\rm max}(E_L)$ for 1040 nm and NA = 0.8. The $R_{\rm max}$ values are calculated from measured $T_{\rm osc}$ values using the Gilmore model. The upper inset in Fig. 2 shows the ratio $R_{\rm max}$(Gilmore)/$R_{\rm max}$(Rayleigh) as a function of $T_{\rm osc}$. For the shortest oscillation times observed in our study, the actual bubble radius is almost twice as large as predicted by the Rayleigh model. For the photographic determination of $R_{\rm max}$, images were taken at time $T_{\rm osc}/2$ to capture the bubble at the stage of maximum expansion. We find excellent agreement between the results of both methods for radii larger than the optical resolution limit $d = 1.22\ \lambda/{\rm NA}$. However, the light scattering technique provided reliable results down to much smaller bubble sizes.

In our theoretical analysis of fs laser-driven bubble formation [1], we first calculate the dependence of free-electron density $\rho_{\rm max}$ at the end of the laser pulse on irradiance I using a rate equation model. Multiplication of $\rho_{\rm max}$ by the average energy of a free electron then yields the volumetric energy density $\varepsilon = \rho_{\rm max}(\tilde{\Delta} + \bar{E}_{\rm kin})$, where $\tilde{\Delta}$ is the ionization potential, and $\bar{E}_{\rm kin} = (5/4)\tilde{\Delta}$ is the average kinetic energy of the free electrons [1]. The temperature rise produced by thermalization of the free-electron energy is given by $\Delta T = \varepsilon/(\rho_0 C_p)$, where C_p is the heat capacity and ρ_0 the mass density of the medium, and the final temperature is $T = 20\,^{\circ}{\rm C} + \Delta T$. We take an ellipsoidal temperature distribution $T(x, y, z) \propto \rho_{\rm max}(x, y, z)$ as starting point for the calculation of the thermoelastic stress evolution. Because of the predominance of multiphoton ionization, the $\rho(I)$ dependence is, in this distribution, simplified to $\rho_{\rm max} \propto I^k$. When the compressive stress in the focus center relaxes, a tensile

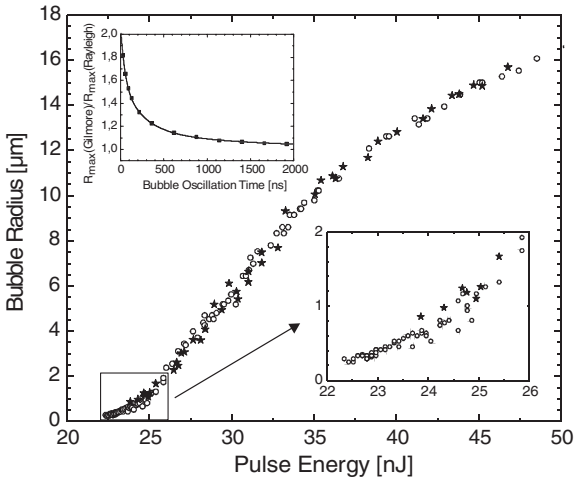

FIG. 2. Bubble radii $R_{\rm max}$ at $\lambda = 1040$ nm, NA = 0.8 determined from the light scattering signals (○) and photographs (★). The inset shows $R_{\rm max}$(Gilmore)/$R_{\rm max}$(Rayleigh) as a function of $T_{\rm osc}$ (see text).

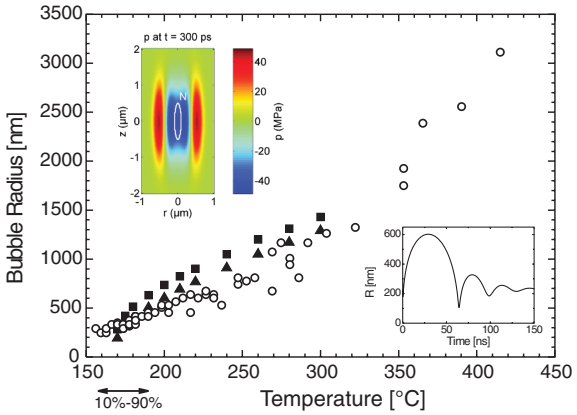

FIG. 3 (color). Measured bubble radii R_{max} (○) compared to predictions for isothermal (■) and adiabatic (▲) conditions of the bubble content with respect to the surrounding liquid. All data refer to 1040-nm pulses focused at NA = 0.8. Arrows mark the region from 10% to 90% breakdown probability. The insets show the calculated thermoelastic stress distribution with bubble nucleus (N), and the adiabatic bubble oscillation for a peak temperature of $T = 200\,^{\circ}\mathrm{C}$.

wave evolves that results in a phase change once the tensile stress amplitude exceeds the stability limit (rupture threshold) of the superheated water. We assume that this occurs in the entire volume in which the kinetic spinodal limit as defined by Kiselev [2] is exceeded. This volume is taken as bubble nucleus, and the subsequent dynamics driven by tensile stress and vapor pressure inside the bubble is calculated using the Gilmore model [13]. The influence of heat exchange between bubble content and surrounding liquid is assessed by distinguishing between isothermal and adiabatic conditions. Figure 3 shows the numerical results for 1040 nm and NA = 0.8. Assuming a thermalization time of 10 ps [10,15], we obtain a threshold temperature and pressure of $T_{th} = 167.7\,^{\circ}\mathrm{C}$ and $p_{th} = -62.8$ MPa. Results for T_{th} are largely independent of wavelength because the shape of the focal irradiance distribution remains the same. However, with increasing NA, the focus becomes less elongated, the tensile stress wave more strongly focused, and T_{th} decreases to $151.5\,^{\circ}\mathrm{C}$ at NA = 1.3 [1].

In Fig. 2, the experimental threshold for 50% probability of bubble formation is $E_{th} = 22.6$ nJ. It corresponds to $I_{th} = 3.37 \times 10^{12}$ W/cm^2 if diffraction-limited focusing is assumed. According to our plasma model, this irradiance results in a free-electron density of $\rho_{max} = 0.346 \times 10^{21}$ cm^{-3} at the focus center and a peak focus temperature of $233\,^{\circ}\mathrm{C}$. This temperature agrees fairly well with the bubble formation threshold $T_{th} = 167.7\,^{\circ}\mathrm{C}$ predicted by our theory of thermoelastic bubble formation. However, for the critical plasma density, our plasma model yields temperatures ranging from $666\,^{\circ}\mathrm{C}$ for $\lambda = 1040$ nm with $\rho_{cr} = 1.03 \times 10^{21}$ cm^{-3} to $5838\,^{\circ}\mathrm{C}$ for $\lambda = 347$ nm with $\rho_{cr} = 9.28 \times 10^{21}$ cm^{-3}. These values far exceed the bubble formation threshold and exhibit a wavelength dependence that is not expected for a phase transition temperature. We conclude that ρ_{cr} is an inappropriate criterion for comparison with measured threshold data because it relates to a change in laser-plasma coupling rather than to the phase transition underlying bubble formation.

To compare the experimental $R_{max}(E_L)$ values with model predictions for $R_{max}(T)$, we equate the experimental and theoretical thresholds E_{th} and T_{th}, and transform the E_L scale into a temperature scale as described above. As shown in Fig. 3, we obtain an excellent agreement between predicted and measured bubble radii at the bubble formation threshold. With increasing temperature, the theoretical R_{max} values grow initially slightly faster than the measured ones because we calculate the bubble expansion using the stress evolution in the focus center that originates in a situation without bubble formation. This approach neglects the clipping of the tensile stress amplitude upon rupture of the liquid, and overrates the force acting on the bubble wall that is actually located at a distance from the focus center.

Under isothermal conditions, when temperature T_B and vapor pressure p_v inside the bubble decay only by heat diffusion within the liquid surrounding the bubble, R_{max} is only slightly larger than under adiabatic conditions, when T_B and p_v drop rapidly upon bubble expansion (Fig. 3). The adiabatic bubble motion is, in turn, almost identical to the case where p_v is not at all taken into account (not shown). We conclude that, near threshold, fs laser-induced bubble formation is largely driven by tensile thermoelastic stress with little contribution from vapor pressure. However, for $T > 300\,^{\circ}\mathrm{C}$, a steep increase of R_{max} is observed, corresponding to the increase in Fig. 2 for $E_L > 25$ nJ that starts about 11% above E_{th}. Since at $T \approx 300\,^{\circ}\mathrm{C}$ the spinodal limit is crossed at ambient pressure [16], no tensile stress is required any more for $T > 300\,^{\circ}\mathrm{C}$ to induce a phase transition, and bubble formation progresses as explosive vaporization.

TABLE I. Threshold for fs optical breakdown in water (340 fs) at different wavelengths λ and NA, with focal radius $r = 0.61\,\lambda/\mathrm{NA}$. The threshold values include the breakdown energy E_{th} (50% breakdown probability), irradiance I_{th}, threshold sharpness $S = E_{th}/\Delta E$ where ΔE denotes the interval between 10% and 90% breakdown probability, and the bubble size R_{max} at threshold.

λ [nm]	NA	r [nm]	E_{th} [nJ]	I_{th} [10^{12} W/cm^2]	S	R_{max} [nm]
1040	0.8	793	22.6	3.37	30.5	328 ± 44
1040	0.9	705	18.5	3.49	18.9	322 ± 96
520	0.8	397	4.79	2.85	62.3	288 ± 28
520	0.9	353	4.20	3.17	67.8	232 ± 17
347	0.8	264	3.95	5.29	47.1	216 ± 17
347	0.9	235	3.78	6.40	52.2	190 ± 9

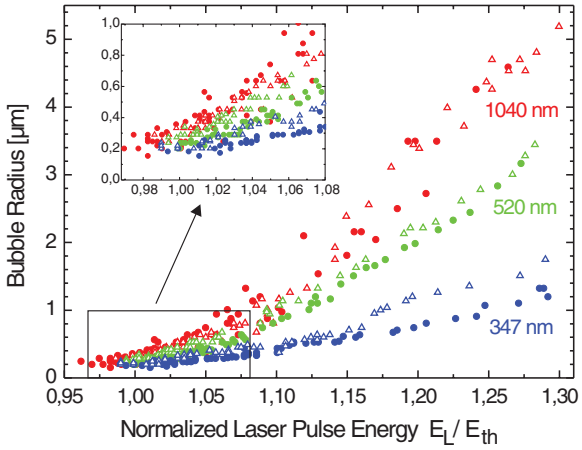

FIG. 4 (color). Bubble radius R_{max} as a function of dimensionless pulse energy E_L/E_{th} for different wavelengths at NA = 0.9 (●) and NA = 0.8 (△).

Threshold data for fs-laser-induced nanocavitation at various wavelengths are summarized in Table I. The mean bubble size at threshold ranges from 190 nm (UV) to 320 nm (IR) for NA = 0.9 which is smaller than the diffraction-limited focus diameter. Bubbles will be even smaller for larger NAs and in cells where they are confined by the cytoskeleton [5]. At threshold, only a small fraction ($\approx 0.0002\%$) of the laser energy E_L is converted into bubble energy E_B because most light is transmitted through the focus. Moreover for $T = 200°C$, NA = 0.8 only 0.46% of the absorbed energy is converted from heat into thermoelastic energy from which 7.2% are further transformed into E_B [1].

The breakdown probability increases from 10% to 90% within a very small energy range ΔE; i.e., the threshold sharpness measured by $S = E_{th}/\Delta E$ assumes large values. The highly predictable onset of nanocavitation corroborates our theoretical assumption that bubble formation is not initiated by inhomogeneous nucleation in the superheated water but rather by a crossing of the well-defined kinetic spinodal limit [2]. The irradiance threshold I_{th} is largest for UV breakdown, in spite of the low order of multiphoton processes, because the avalanche ionization rate decreases strongly with decreasing wavelength [1].

Figure 4 shows the nanocavitation range for all investigated parameters. Apparently, near-UV wavelengths are best suited for nanosurgery because R_{max} is smallest at threshold and increases most slowly with E_L. The low order of multiphoton processes at short wavelengths translates into a slow increase of ρ_{max} and, consequently, R_{max} with E_L, which provides a good adjustability of the surgical effect. Nevertheless, the $R_{max}(E_L)$ dependence is generally quite strong, and for $E_L = 2E_{th}$, R_{max} already resembles the size of a biological cell (Fig. 2). An online control of bubble size could thus further improve the surgical precision.

In conclusion, we found that bubbles produced by fs optical breakdown in water are, at threshold, smaller than the diffraction-limited focus diameter. Experimental results support a model of bubble formation in heated and thermoelastically stretched liquids that predicts a threshold temperature of $\approx 168\,°C$. For $T > 300\,°C$, bubble expansion is driven by a phase explosion. Incorporation of bubble formation into the modeling of fs breakdown permits a more reasonable comparison with experimental thresholds than the criterion that a critical free-electron density must be exceeded above which plasma becomes reflective. UV laser pulses produce the smallest bubbles and offer the broadest working range for nanocell surgery.

This work was supported by U.S. Air Force Office of Scientific Research, and German Bundesministerium für Bildung und Forschung.

*Corresponding author.
vogel@bmo.uni-luebeck.de
†guenther.paltauf@uni-graz.at

[1] A. Vogel, J. Noack, G. Hüttmann, and G. Paltauf, Appl. Phys. B **81**, 1015 (2005).
[2] S. B. Kiselev, Physica (Amsterdam) **269A**, 252 (1999).
[3] A. Vogel, S. Busch, and U. Parlitz, J. Acoust. Soc. Am. **100**, 148 (1996).
[4] V. Venugopalan, A. Guerra, K. Nahen, and A. Vogel, Phys. Rev. Lett. **88**, 078103 (2002).
[5] M. S. Hutson and X. Ma, Phys. Rev. Lett. **99**, 158104 (2007).
[6] J. Noack, D. X. Hammer, G. D. Noojin, B. A. Rockwell, and A. Vogel, J. Appl. Phys. **83**, 7488 (1998).
[7] C. B. Schaffer, A. Brodeur, J. Garcia, and E. Mazur, Opt. Lett. **26**, 93 (2001).
[8] C. Arnold, A. Heisterkamp, W. Ertmer, and H. Lubatschowski, Opt. Express **15**, 10303 (2007).
[9] A. Vogel, K. Nahen, D. Theisen, R. Birngruber, R. J. Thomas, and B. A. Rockwell, Appl. Opt. **38**, 3636 (1999).
[10] C. B. Schaffer, N. Nishimura, E. N. Glezer, A. M. T. Kim, and E. Mazur, Opt. Express **10**, 196 (2002).
[11] B. P. Barber, R. A. Hiller, R. Löfstedt, S. J. Putterman, and K. R. Weninger, Phys. Rep. **281**, 65 (1997).
[12] Lord Rayleigh, Philos. Mag. **34**, 94 (1917).
[13] F. R. Gilmore, Calif. Inst. of Tech. Hydrodyn. Lab. Report No. 26-4 (1952).
[14] National Institute of Standards: http://webbook.nist.gov/chemistry/fluid (2005).
[15] C. Sarpe-Tudoran, A. Assion, M. Wollenhaupt, M. Winter, and T. Baumert, Appl. Phys. Lett. **88**, 261109 (2006).
[16] A. Vogel and V. Venugopalan, Chem. Rev. **103**, 577 (2003).